Journal of Nano- and Electronic Physics
Vol. **18** No 2, 02029(8pp) (2026)

Журнал нано- та електронної фізики
Том **18** № 2, 02029(8cc) (2026)

OPEN ACCESS

REGULAR ARTICLE

Application of Iron Nanoparticles for the Remediation of Chromium

Andrew Kotsyubynsky[1,*], Halyna Hrytsuliak[1], Mariia Liaskovska[1,2], Vasyl Vytvytskyi[1], Oleg Turchyn[1], Yulia Kotsyubynska[2], Natalia Kozan[2], Hanna Ersteniuk[2]

[1] *Ivano-Frankivsk National Technical University of Oil and Gas, Ivano-Frankivsk, Ukraine*
[2] *Ivano-Frankivsk National Medical University, Ivano-Frankivsk, Ukraine*

(Received 21 January 2026; revised manuscript received 14 April 2026; published online 29 April 2026)

Soil contamination with chromium poses a serious threat to the environment and human health due to its toxicity and persistence. This study evaluates the effectiveness of iron-containing nanoparticles for the remediation of chromium-contaminated soils. Two types of iron nanoparticles synthesized and investigated: nanosized zero-valent iron (nZVI) and nano-magnetite (nFe_3O_4). Soil samples were mixed with nanoparticles at different doses, homogenized and incubated under controlled conditions for 10, 20, 30, 60 and 90 days. For each sampling time, chromium concentration and its leachability were analyzed. Chemical and phase composition analysis investigated by X-ray diffraction spectroscopy, atomic absorption spectroscopy and X-ray fluorescence analysis. Treatment with both types of iron nanoparticles showed a significant decrease in Cr concentration in aqueous extracts compared to the control samples. The leachability of Cr in the treated soil samples also decreased significantly and remained stable throughout the experiment. The results indicate that nZVI immobilized Cr by adsorption of Cr(VI) on the shell with its reduction to Cr(III). The interaction mechanism between nFe_3O_4 and Cr(VI) involved both adsorption [1], and reduction, although its reduction capacity was lower than that of nZVI. Analytical methods confirmed the change in soil chemical composition after treatment and separation of iron nanoparticles. This study demonstrates that iron-containing nanoparticles can effectively remediate chromium-contaminated soils under different environmental conditions.

Keywords: Magnetite, Chromium reduction, Soil pollution, Zero-valent iron, Nanoreduction.

DOI: 10.21272/jnep.18(2).02029 PACS numbers: 78.67.Bf, 91.62.Rt

1. INTRODUCTION

Soil pollution is a significant global problem due to its detrimental effects on the ecosystem, threatening food security and human health. Among the various soil pollutants [2], heavy metals are of particular concern due to their extremely long-term biodegradability, persistence and toxicity. Chromium (Cr) is widely used in industrial processes including metallurgy, leather tanning, wood processing, electroplating and oil refining, leading to its widespread presence in the environment.

Chromium in soil exists primarily in two oxidation states: Cr(III) and Cr(VI). While Cr(III) occurs in relatively insoluble oxides and hydroxides of cations, Cr(VI) exists as oxoanions that are repelled by negatively charged soil particles, remaining mobile in the soil solution and readily available to plants and soil organisms. As a result, Cr(VI) is highly bioavailable and is considered hundreds of times more toxic than Cr(III). [3]

Traditional technologies for remediation of chromium-contaminated soils include electrokinetic remediation, soil washing, phytoremediation, and chemical stabilization. [4] However, these methods often have limitations in terms of efficiency, cost-effectiveness and environmental impact. [5] Recently, nanotechnology has emerged as a promising approach to soil remediation, offering advantages such as high reactivity, large surface area, and the possibility of targeted treatment.

Iron-based nanoparticles are particularly effective for chromium reduction due to their ability to reduce toxic Cr(VI) to less toxic Cr(III) and their ability to adsorb metal pollutants [6]. This study discusses two types of iron nanoparticles that have shown promise for chromium reduction: nanosized zero-valent iron (nZVI) and magnetite nanoparticles (nFe_3O_4). Nanosized zero-valent iron (nZVI) has a core-shell structure consisting of metallic iron (Fe^0) in the core surrounded by a shell of iron oxide/hydroxide. The core is responsible for the reduction processes, while the shell facilitates the adsorption and electron transfer. [7] This dual functionality makes nZVI effective for both Cr(VI) reduction and Cr immobilization. [8]. Magnetite nanoparticles (nFe_3O_4) have a high adsorption capacity for heavy metals and have the advantage of magnetic properties. [9] This makes them easy to separate after use.

This study aims to evaluate and compare the effectiveness of nZVI and nFe_3O_4 for the remediation of chromium-contaminated soils, with a focus on their ability to reduce the mobility and bioavailability of chromium.

2. MATERIALS AND METHODS

2.1 Synthesis and Characterization Techniques of nFe_3O_4 and nZVI

* Correspondence e-mail: andriy.kotsyubynsky@nung.edu.ua

Cite this article as: A. Kotsyubynsky et al., *J. Nano- Electron. Phys.* 18 No 2, 02029 (2026) https://doi.org/10.21272/jnep.18(2).02029

Analytical pure materials were used to synthesize the nanoparticles described in this study. Zero-valent iron nanoparticles were synthesized by chemical reduction of iron(III) ions using sodium borohydride.

The reaction proceeded according to the following scheme:

$$4Fe^{3+} + 3BH_4^- + 9H_2O \rightarrow$$
$$\rightarrow 4Fe^0 + 3H_2BO_3^- + 12H^+ + 6H_2$$

The nZVI particles were separated using a permanent neodymium magnet, washed three times with deoxygenated deionized water and once with ethanol, and then dried under vacuum at room temperature for 24 hours. The dried nZVI particles were stored in sealed containers under nitrogen until use.

Magnetite nanoparticles were synthesized by the co-precipitation method. [10]

Magnetite nanoparticles were created according to the reaction:

$$Fe^{2+} + 2Fe^{3+} + 8OH^- \rightarrow Fe_3O_4 + 4H_2O$$

The particles were dried under vacuum at 60 °C for 12 hours and stored in sealed containers. The synthesized nanoparticles were characterized using various analytical methods to determine their size, structure, and composition [11].

2.2 Characterization Techniques

X-ray diffraction (XRD) spectra were obtained on a Shimadzu XRD-7000 diffractometer using Cu Kα radiation in the diffraction angle range (2θ) from 5° to 90° with a step of 0.04° to identify the crystalline phases of the nanoparticles.

X-ray fluorescence analysis (XRF) was performed using a wave-dispersive X-ray fluorescence spectrometer X-ray fluorescence analyzer EXPERT 3L [12] to determine the elemental composition of nanoparticles. The research was conducted in an atmosphere of ultra-pure helium. The research error was 10 ppm [13].

Flame atomic absorption spectrometry (FAAS) was performed on an Avio 550/560 instrument.

Soil samples were collected from an industrial area in Kalush with a history of chromium contamination. The samples were taken from the surface layer (0-30 cm), air-dried, and sieved through a 2 mm mesh sieve to remove coarse particles. The soil was characterized for various physicochemical properties according to standard methods. [14]

The total concentration of chromium and other heavy metals (Cd, Cu, Ni, Pb, Zn, etc.) in the soil was determined by acid-base analysis followed by FAAS analysis on an Avio 550/560 instrument. Additionally, the soil was analyzed by X-ray fluorescence and X-ray diffraction analysis to determine its elemental composition and phase composition before and after treatment with iron nanoparticles.

The specific surface area of the synthesized nanoparticles was determined with the low-temperature nitrogen adsorption-desorption method by Quantachrome NOVA 2200e two-station gas analyzer. Measurements performed at liquid nitrogen temperature (77 K). Before analysis, samples weighing 0.15-0.20 g degassed at 120 °C for 4 hours in a helium stream to remove adsorbed moisture and gases. The specific surface area was calculated by the Brunauer-Emmett-Teller (BET) method in the range of relative pressures P/P_0 = 0.05-0.30. The total pore volume was determined at P/P_0 = 0.99. The pore size distribution was calculated by the BJH (Barrett-Joyner-Halenda) method using the desorption branch of the isotherm.

2.3 Experiments under Static Conditions

Soil samples (15 g) were placed in plastic tubes (50 ml) and mixed with iron nanoparticles (nZVI or nFe_3O_4) at different doses. The nZVI nanoparticles were added at 20 g Fe/kg soil, while the nFe_3O_4 was added at 36.2 g Fe/kg soil, based on previous tests. Control samples without the addition of nanoparticles were also prepared.

35 ml of deionized water was added to each tube to create pseudoanaerobic conditions and minimize oxidation of the nanoparticles, after thoroughly mixing the soil with the nanoparticles. The tubes were capped and incubated at 28 °C in a controlled environment chamber (thermostat) in the dark for 10, 20, 30, 60 and 90 days. During the first 24 hours, the tubes were periodically depressurized to release gas evolved during the reactions of the nanoparticles.

For each sampling time (10, 20, 30, 60 and 90 days), the tubes were centrifuged at 3000 rpm for 10 minutes to separate the aqueous phase from the soil. The liquid phase collected, filtered through a 0.45 μm membrane filter and analyzed for chromium content. The soil samples were air-dried and used to determine Cr(VI) concentration and chromium leachability. All experiments were performed in triplicate [15].

2.4 Analytical Methods for the Chromium Determination

The total chromium concentration in the aqueous phase determined by flame atomic absorption spectrometry (FAAS) on an Avio 550/560 instrument with an air-acetylene flame at a wavelength of 357.9 nm. Calibration standards were prepared from 1000 mg/L chromium standard solution.

The concentration of Cr(VI) in soil samples was determined by ion chromatography with UV-visible detection. Soil samples (0.1 g) were mixed with 5 mL of 50 mM nitric acid, 10 mL of eluent (containing 2 mM pyridine-2,6-dicarboxylic acid, 2 mM sodium dihydrogen phosphate, 10 mM sodium iodide, 50 mM ammonium acetate, and 2.8 mM lithium hydroxide) and 10 μL of concentrated nitric acid. The mixture heated for 30 min, cooled to room temperature, filtered, and analyzed by ion chromatography.

The leachability of chromium in soil samples assessed using the Toxic Characterization Leaching Procedure (TCLP) according to USEPA Method 1311. Soil samples (1 g) extracted with 20 mL of sodium acetate buffer (pH 4.93 ± 0.05) by shaking for 18 hours. The extracts filtered and analyzed for chromium concentration by FAAS.

To determine the bioavailable forms of chromium, the TCLP method was used according to the EPA 1311 protocol, which simulates leaching conditions in an acidic environment and allows to estimate the potential

mobility of chromium in the soil. Additionally, the determination of Cr(VI) was carried out by alkaline extraction using 0.1M Na_2CO_3/0.1M NaOH followed by colorimetric analysis with diphenylcarbazide, which allows to selectively determine the most toxic form of chromium.

X-ray fluorescence (XRF) analysis of the soil performed before and after treatment and separation of iron nanoparticles to assess changes in chemical composition. The soil samples dried, ground to a powder state, and analyzed using an XRF spectrometer.

Statistical analysis performed using Statistica 12. Data tested for normality using the Kolmogorov-Smirnov test. Differences between treatments were determined using one-way analysis of variance (ANOVA) at a significance level of $p < 0.05$, followed by Tukey's post-hoc test for multiple comparisons.

3. RESULTS AND DISCUSSION

3.1 Textural Characteristics of Synthesized Nanoparticles

The results of BET analysis of the synthesized nanoparticles are given in Table 1. The nFe_3O_4 nanoparticles were characterized by a significantly higher specific surface area (78.4 ± 2.3 m^2/g) compared to nZVI (32.6 ± 1.8 m^2/g). This pattern is consistent with the X-ray diffraction results, according to which the average crystallite size of nFe_3O_4 (20-30 nm) is smaller than that of nZVI (25-35 nm). Both types of nanoparticles exhibited a mesoporous structure with an average pore diameter of 8.2 ± 0.5 nm for nZVI and 5.7 ± 0.4 nm for nFe_3O_4.

The results of BET analysis of the synthesized nanoparticles are given in Table 1. The nFe_3O_4 nanoparticles show a significantly higher specific surface area (78.4 ± 2.3 m^2/g) compared to nZVI (32.6 ± 1.8 m^2/g). This pattern correlates with the X-ray diffraction results, according to which the average crystallite size of nFe_3O_4 (20-30 nm) is smaller than that of nZVI (25-35 nm). Both types of nanoparticles exhibited a mesoporous structure with an average pore diameter of 8.2 ± 0.5 nm for nZVI and 5.7 ± 0.4 nm for nFe_3O_4.

Nitrogen adsorption-desorption isotherms for both types of nanoparticles (Fig. 1) belong to type IV according to the IUPAC classification, which is typical for mesoporous materials. The hysteresis loop of type H3 indicates the presence of particle aggregates with slit-like pores formed as a result of agglomeration of nanoparticles. The pore size distribution curves (Fig. 6) demonstrate a unimodal distribution with a maximum at 8 nm for nZVI and 5-6 nm for nFe_3O_4. Despite the larger specific surface area of nFe_3O_4, the experimentally established higher efficiency of chromium removal by nZVI nanoparticles is explained by their significantly stronger reducing ability, due to the presence of the Fe^0 metal core. Thus, for the chromium remediation process, the chemical activity of nanoparticles is a more determining factor than their surface area.

3.2 Characterization of Iron Nanoparticles by XRD

XRD analysis allowed us to determine the average crystallite size of the synthesized nanoparticles using the peak width at half-maximum intensity (FWHM) calculated using the Scherrer formula. For nZVI nanoparticles, the average crystallite size was 25-35 nm, while for nanomagnetite (nFe_3O_4 this figure was 20-30 nm).

Table 1 – Textural characteristics of synthesized nanoparticles according to BET analysis (Quantachrome NOVA 2200e)

Parameter	nZVI	nFe_3O_4
Specific surface area, S_BET (m^2/g)	32.6 ± 1.8	78.4 ± 2.3
Total pore volume, V_total (sm^3/g)	0.067 ± 0.004	0.112 ± 0.006
Micropore volume, V_micro (sm^3/g)	0.003 ± 0.001	0.008 ± 0.001
Average pore diameter according to BJH, Dpore (nm)	8.2 ± 0.5	5.7 ± 0.4
Crystallite size, XRD (nm)	25-35	15-25
Isotherm type (IUPAC)	IV	IV
Hysteresis loop type	H3	H3
BET constant, C	86	124

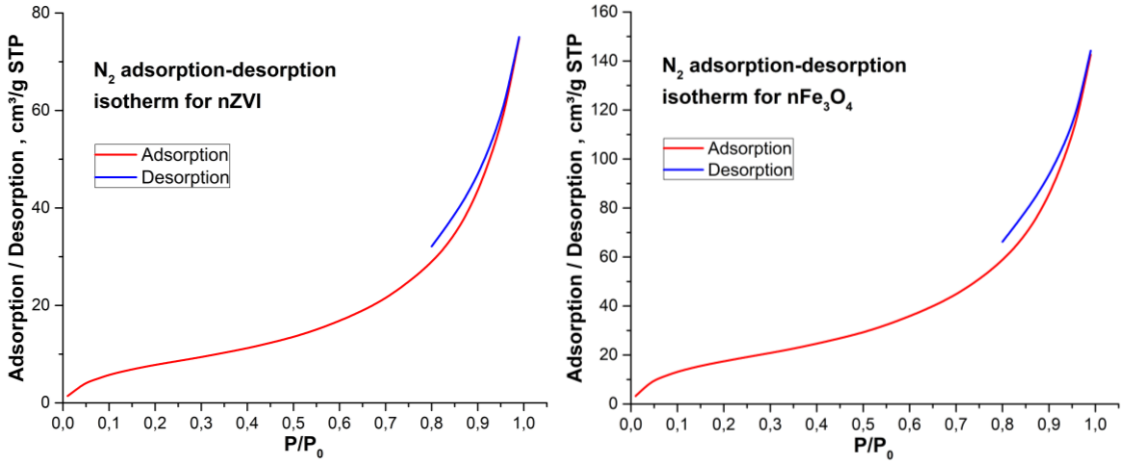

Fig. 1 – N_2 adsorption-desorption isotherm for nZVI and nFe_3O_4 nanoparticles

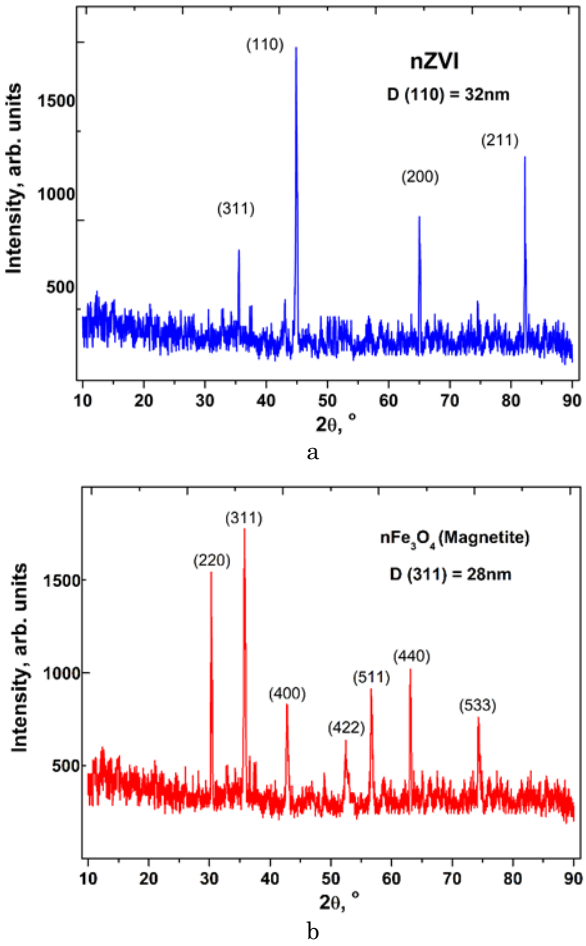

Fig. 2 – X-ray diffraction spectrum of synthesized nZVI (a) and nFe_3O_4 (b) nanoparticles

The X-ray diffraction spectra of the synthesized nanoparticles shown in Figure 2. The XRD spectrum of nZVI showed characteristic peaks at 2θ values of 44.7°, 65.0° and 82.3°, corresponding to the (110), (200) and (211) planes of α-Fe^0 (ICDD 04-013-5208), respectively. The weaker peak at 35.5° attributed to iron oxide (Fe_3O_4/Fe_2O_3) on the surface of the nanoparticles, confirming the core-shell structure of nZVI.

The nFe_3O_4 nanoparticles showed characteristic diffraction peaks at 2θ values of 30.3°, 35.7°, 43.3°, 53.8°, 57.3°, 63.1° and 74.3°, which are consistent with standard data for magnetite (ICDD 04-013-9808).

3.3 Characterization of Iron Nanoparticles by XRF Method

XRF analysis confirmed the elemental composition of the nanoparticles. The nZVI particles contained 94.2 % Fe with trace amounts of other elements, while the nFe_3O_4 particles contained 72.3 % Fe and 27.1 % O, which is close to the theoretical composition of magnetite (72.4 % of Fe and 27.6 % of O).

3.4 Soil Characteristics

The physical and chemical properties of the experimental soil summarized in Table 2. The soil had a sandy loam texture with a pH of 6.29 and an electrical conductivity of 2.7 dS/m. The organic matter content was relatively low (0.81 %), and the soil contained moderate amounts of exchangeable cations. The total chromium concentration in the soil was 214 mg/kg, Cr(VI) was 65 mg/kg. According to regional screening levels, this soil considered contaminated and requires remediation.

XRF analysis of the soil before treatment showed that the soil contained chromium (0.021 %) and other elements: silicon (56.3 %), aluminum (14.2 %), calcium (9.8 %), iron (2.3 %), potassium (1.9 %), magnesium (1.5 %), sodium (0.8 %), titanium (0.6 %) and trace amounts of other elements.

Table 2 – Physicochemical properties of the experimental soil

pH	Ca mg/kg	Mg mg/kg	Na mg/kg	K mg/kg	Cr mg/kg	Cr(VI) mg/kg	Cu mg/kg	Pb mg/kg	Zn mg/kg	Sand %	Silt %	Clay %
6.29	594	90	31	155	214	65	9.1	10	30	64	25	11

Methods: Standard protocols applied. Texture: Sandy clay loam [16]

3.5 The Effect of Iron Nanoparticles on Chromium in Aqueous Soil Extract

In the control samples, chromium concentrations remained relatively high and stable throughout the experiment, averaging about 19.5 mg/L. This indicates that a significant portion of the soil chromium was mobile and potentially bioavailable. The addition of iron nanoparticles significantly reduced the chromium concentration in the aqueous extract at all sampling times. After 10 days of treatment, the chromium concentration in the nZVI-treated samples decreased by 75.4 %, and in the nFe_3O_4-treated samples by 68.2 % respectively. Chromium removal efficiency increased over time for both types of nanoparticles.

According to atomic absorption spectrometry, after 90 days of treatment, the chromium removal efficiency reached 96.4 % for nZVI and 94.2 % for nFe_3O_4 respectively. X-ray fluorescence analysis, which reflects the total element content in the solid phase, showed a reduction in chromium content of 63.6 % for nZVI and 47.6 % for nFe_3O_4 after 90 days.

The difference in effectiveness between the two types of nanoparticles was statistically significant ($p < 0.05$), indicating a higher effectiveness of nZVI compared to nFe_3O_4 in reducing the mobility of chromium in the soil. This can be explained by the stronger reducing capacity of zero-valent iron compared to magnetite, which leads to a more efficient reduction of Cr(VI) to Cr(III), which is less mobile and less toxic. The results indicate that the main mechanism of action of iron nanoparticles is not the physical removal of chromium from the soil, but the conversion of toxic soluble Cr(VI) to insoluble Cr(III), which remains in the soil in a form inaccessible to living organisms. The interaction occurred according to the reaction:

$$CrO_4^{2-} + 3Fe^0 + 8H^+ \rightarrow Cr^{3+} + 3Fe^{2+} + 4H_2O$$

This mechanism ensures stable immobilization of chromium throughout the entire experiment.

3.6 The Effect of Iron Nanoparticles on Chromium Leachability

The leachability of chromium in soil determined by the TCLP test is shown in Figure 3. The TCLP leachable chromium in the control samples ranged from 5.9 to 7.5 mg/kg, indicating a potential environmental risk. Treatment with iron nanoparticles significantly reduced the leachability of chromium to levels between 1.1 and 1.7 mg/kg, representing a reduction of 71-82 %. No significant differences in chromium leachability were observed between the two types of iron nanoparticles, and there was no significant change in leachability over time for either treatment. This indicates that the immobilization of chromium by iron nanoparticles was stable over the 90-day experimental period.

Reduction of chromium leachability is an important indicator of treatment effectiveness because it reflects the potential for chromium release into the environment under acidic conditions that may occur in landfills or through acid rain.

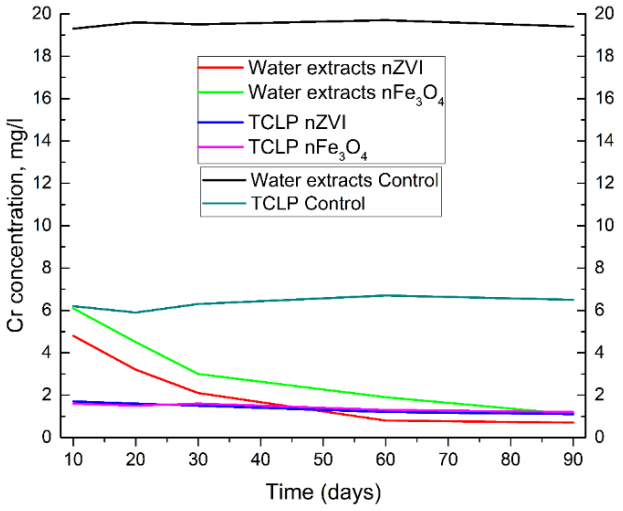

Fig. 3 – Average Cr concentration (mg/L) in aqueous extracts and in TCLP extracts after treatment with iron nanoparticles at different sampling times

3.7 The Effect of Iron Nanoparticles on the Concentration of Cr(VI) in Soil

The Cr(VI) concentration in soil samples after treatment with iron nanoparticles is presented in Figure 4. The initial Cr(VI) concentration in the soil was 65 mg/kg. In the control samples, the Cr(VI) concentration decreased slightly over time to approximately 50 mg/kg after 90 days, possibly due to natural reduction processes in the soil.

The nZVI treatment resulted in a significant reduction in Cr(VI) concentration to approximately 6-7 mg/kg, representing a reduction of approximately 90 %. This level remained stable throughout the 90-day experimental period. Soil samples treated with nFe_3O_4 showed a more moderate reduction in Cr(VI) concentration, reaching levels of 8.5-10.5 mg/kg (approximately 85 % reduction).

The higher efficiency of nZVI in Cr(VI) reduction compared to nFe_3O_4 can be explained by the stronger reducing ability of zero-valent iron. The core of nZVI particles consists of Fe^0, which can directly reduce Cr(VI) to Cr(III) according to the reaction:

$$Cr_2O_7^{2-} + 6Fe^0 + 14H^+ \rightarrow 2Cr^{3+} + 6Fe^{2+} + 7H_2O$$

In the case of nFe_3O_4, the reduction of Cr(VI) is provided by Fe(II) present in the magnetite structure ($Fe(II)Fe(III)_2O_4$). However, the reduction capacity of Fe(II) is lower than that of Fe^0, resulting in less efficient reduction of Cr(VI). The results indicate that nZVI is particularly effective for the remediation of soils contaminated with Cr(VI), while nFe_3O_4 offers a moderate level of reduction with the added advantage of magnetic separation capability.

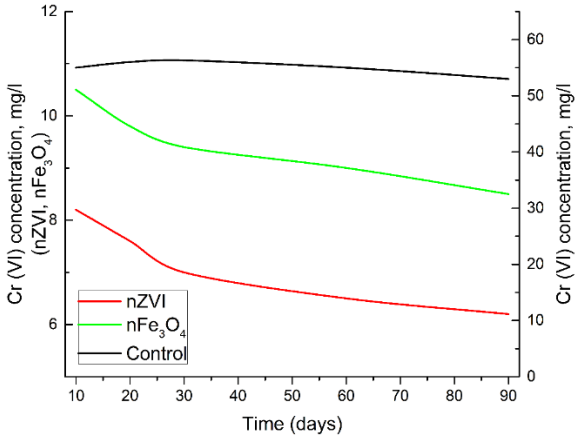

Fig. 4 – Average Cr(VI) concentration (mg/l) in soil samples after treatment with iron nanoparticles at different sampling times

3.8 Comparative Analysis of FAAS and XRF Results

X-ray fluorescence analysis of soil samples before and after treatment with iron nanoparticles provided additional information about changes in soil chemical composition. After 90 days of nanoparticle treatment, soil iron content increased from an initial level of 2.3 % to 9.8 % in samples treated with nZVI and to 7.2 % in samples treated with nFe_3O_4.

Comparison of the results of atomic absorption spectrometry (FAAS) and X-ray fluorescence analysis (XRF) allows to obtain a comprehensive understanding of the processes of chromium immobilization in soil. The FAAS technique, which involves acid digestion of samples, demonstrates a significantly higher efficiency of chromium removal (68-96 %) compared to XRF (9-64 %). This difference is explained by the fact that FAAS measures mainly bioavailable forms of chromium after extraction, while XRF reflects the total content of elements in the solid phase of the sample without prior chemical treatment. This difference confirms that the main mechanism of action of iron nanoparticles is not the physical removal of chromium from the soil, but the conversion of toxic soluble Cr(VI) into insoluble Cr(III), which remains in the soil in a form inaccessible to living organisms.

The results of both analytical methods are consistent

in observing a higher efficiency of nZVI compared to nFe_3O_4, as well as in revealing a dependence of the efficiency on the interaction time. The comparison of FAAS and XRF data is of particular importance for the practical application of the method, since in the context of soil remediation the critical factor is not so much the complete removal of chromium, but the reduction of its bioavailability and toxicity. In this respect, the FAAS results, which show a significant reduction in the extracted chromium, are more relevant for assessing the success of the remediation than the absolute reduction in the total element content reflected in the XRF results.

Table 3 – Results of FAAS analysis of soil samples before and after treatment with iron nanoparticles

No sample	Type of nanoparticles	Interaction time (days)	Cr concentration before treatment (mg/kg)	Cr concentration after treatment (mg/kg)	Removal efficiency (%)
1	nZVI	10	214.3	52.8	75.4
2	nZVI	20	215.7	34.2	84.1
3	nZVI	30	213.8	21.5	89.9
4	nZVI	60	214.5	14.3	93.3
5	nZVI	90	216.1	7.8	96.4
6	nFe_3O_4	10	215.2	68.4	68.2
7	nFe_3O_4	20	213.6	48.1	77.5
8	nFe_3O_4	30	214.9	31.7	85.2
9	nFe_3O_4	60	215.3	19.2	91.1
10	nFe_3O_4	90	214.0	12.5	94.2

Table 4 – Results of XRF analysis of soil samples before and after treatment with iron nanoparticles

No sample	Type of nanoparticles	Interaction time (days)	Elemental composition before processing (wt%)	Elemental composition after processing (wt%)	Change in Fe content (%)	Cr content reduction (%)
1	nZVI	10	Fe: 2.34; Cr: 0.021; Si: 56.2; Al: 14.3; Ca: 9.7; K: 1.9; Mg: 1.5	Fe: 7.82; Cr: 0.018; Si: 53.4; Al: 13.9; Ca: 9.5; K: 1.8; Mg: 1.4	+234.2	14.3
2	nZVI	20	Fe: 2.31; Cr: 0.022; Si: 56.4; Al: 14.1; Ca: 9.8; K: 1.8; Mg: 1.6	Fe: 8.45; Cr: 0.017; Si: 53.1; Al: 13.8; Ca: 9.6; K: 1.7; Mg: 1.5	+265.8	22.7
3	nZVI	30	Fe: 2.28; Cr: 0.021; Si: 56.5; Al: 14.2; Ca: 9.6; K: 1.9; Mg: 1.5	Fe: 9.13; Cr: 0.014; Si: 52.8; Al: 13.7; Ca: 9.4; K: 1.8; Mg: 1.4	+300.4	33.3
4	nZVI	60	Fe: 2.33; Cr: 0.021; Si: 56.3; Al: 14.0; Ca: 9.9; K: 1.8; Mg: 1.4	Fe: 9.58; Cr: 0.010; Si: 52.5; Al: 13.6; Ca: 9.3; K: 1.7; Mg: 1.3	+311.2	52.4
5	nZVI	90	Fe: 2.35; Cr: 0.022; Si: 56.2; Al: 14.3; Ca: 9.7; K: 1.9; Mg: 1.5	Fe: 9.82; Cr: 0.008; Si: 52.2; Al: 13.5; Ca: 9.2; K: 1.8; Mg: 1.4	+317.9	63.6
6	nFe_3O_4	10	Fe: 2.30; Cr: 0.021; Si: 56.3; Al: 14.2; Ca: 9.8; K: 1.8; Mg: 1.6	Fe: 5.45; Cr: 0.019; Si: 54.1; Al: 14.0; Ca: 9.6; K: 1.7; Mg: 1.5	+137.0	9.5
7	nFe_3O_4	20	Fe: 2.32; Cr: 0.021; Si: 56.2; Al: 14.1; Ca: 9.7; K: 1.9; Mg: 1.5	Fe: 6.18; Cr: 0.018; Si: 53.8; Al: 13.9; Ca: 9.5; K: 1.8; Mg: 1.4	+166.4	14.3
8	nFe_3O_4	30	Fe: 2.29; Cr: 0.022; Si: 56.4; Al: 14.3; Ca: 9.6; K: 2.0; Mg: 1.4	Fe: 6.74; Cr: 0.016; Si: 53.5; Al: 13.8; Ca: 9.5; K: 1.9; Mg: 1.3	+194.3	27.3
9	nFe_3O_4	60	Fe: 2.31; Cr: 0.021; Si: 56.3; Al: 14.2; Ca: 9.7; K: 1.9; Mg: 1.5	Fe: 7.01; Cr: 0.013; Si: 53.3; Al: 13.7; Ca: 9.4; K: 1.8; Mg: 1.4	+203.5	38.1
10	nFe_3O_4	90	Fe: 2.33; Cr: 0.021; Si: 56.1; Al: 14.0; Ca: 9.8; K: 1.8; Mg: 1.6	Fe: 7.23; Cr: 0.011; Si: 53.0; Al: 13.6; Ca: 9.3; K: 1.7; Mg: 1.5	+210.3	47.6

Note: *XRF analysis was performed using an X-ray fluorescence spectrometer. Only major elements are shown. The detection limit for most elements is 0.001 %. The change in Fe content reflects the percentage increase in iron concentration after nanoparticle treatment. The decrease in Cr content is calculated as the percentage decrease in total chromium concentration in the samples after treatment.*

3.9 Mechanisms of Chromium Immobilization by Iron Nanoparticles

Based on experimental results and previous studies, we propose that chromium immobilization by iron nanoparticles involves several mechanisms, primarily adsorption and reduction.

In the case of nZVI, Cr(VI) is first adsorbed on the oxide/hydroxide shell of the nanoparticles through electrostatic attraction and ligand exchange. The adsorbed Cr(VI) is then gradually reduced to Cr(III) by electron transfer from the Fe^0 core.

The reduced Cr(III) can form insoluble Cr(III) hydroxides or be incorporated into the structure of the nanoparticle shell to form mixed Cr-Fe (oxy)hydroxides according to the reaction:

$$(1-x)Fe^{3+} + (x)Cr^{3+} + 2H_2O \rightarrow Fe_{(1-x)}Cr_xOOH + 3H^+$$

This process effectively immobilizes chromium, reducing its bioavailability and leaching potential.

Chromium immobilization for nFe_3O_4 occurs primarily by adsorption on the surface of the nanoparticles, with some reduction of Cr(VI) to Cr(III) by Fe(II) present in the magnetite structure. Adsorption is influenced by electrostatic interactions, as the negatively charged Cr(VI) oxoanions are attracted to the positively charged sites on the magnetite surface at acidic pH. The long-term stability of immobilized chromium is supported by the formation of stable Cr-Fe precipitates and the incorporation of Cr(III) into the iron oxide structure, which is less prone to dissolution and re-oxidation compared to pure Cr(III) hydroxides. Figure 5 shows the X-ray diffraction spectra of separated nZVI and nFe_3O_4 nanoparticles after 90 days of treatment.

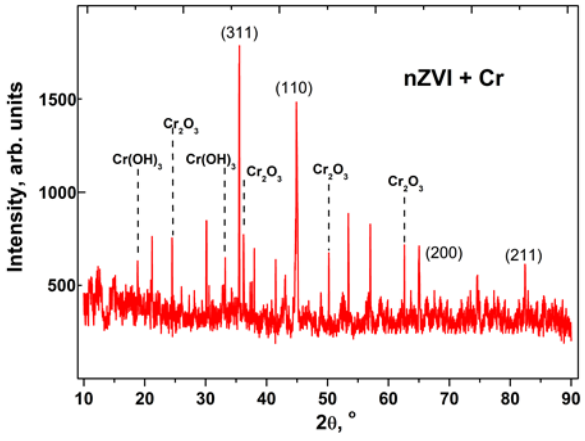

a

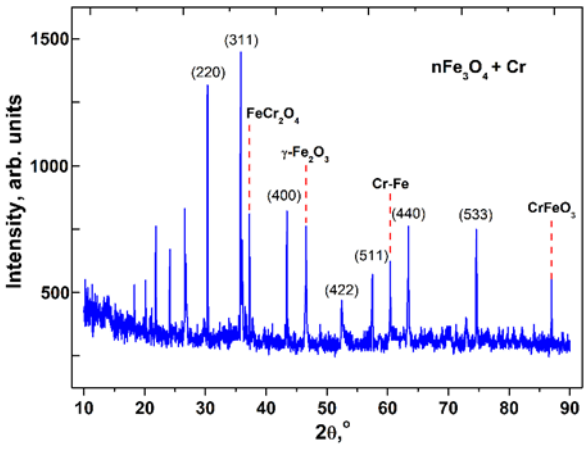

b

Fig. 5 – X-ray diffraction spectra of separated nZVI (a) and nFe_3O_4 (b) nanoparticles after 90 days of treatment

4. CONCLUSIONS

This study demonstrated the effectiveness of two types of iron nanoparticles (nZVI and nFe_3O_4) in remediation of chromium-contaminated soils. Both types of nanoparticles significantly reduced the chromium concentration in the aqueous soil extract and reduced the leachability of chromium. nZVI nanoparticles were more effective in reducing Cr(VI) concentration in soil (96.4 % reduction) compared to nFe_3O_4 (94.2 % reduction) due to the stronger reducing capacity of zero-valent iron.

The immobilization of chromium by iron nanoparticles was stable over a 90-day experimental period, indicating the potential for long-term remediation of chromium-contaminated soils. The main mechanisms of chromium immobilization included adsorption on the surface of the nanoparticles, reduction of Cr(VI) to the less toxic Cr(III), and formation of stable Cr-Fe precipitates. X-ray fluorescence analysis confirmed the changes in the elemental composition of the soil after treatment and separation of iron nanoparticles.

Thus, iron-based nanoparticles, especially nZVI, offer a promising approach for the remediation of chromium-contaminated soils. The choice of nanoparticle type.

REFERENCES

1. T. Tatarchuk, L. Soltys, W. Macyk, *J. Mol. Liquids* **384**, 122174 (2023) https://doi.org/10.1016/j.molliq.2023.122174.
2. M. Liaskovska, T. Tatarchuk, V. Kotsyubynsky, *Phys. Chem. Solid State* **26** No 2, 216 (2025) https://doi.org/10.15330/pcss.26.2.216-230.
3. P. Sharma, S.P. Singh, S.K. Parakh, Y.W. Tong, *Bioengineered* **13** No 3, 4923 (2022) https://doi.org/10.1080/21655979.2022.2037273.
4. V. Lopushnyak, H. Hrytsuliak, I. Kozova, T. Jakubowski, Y. Kotsyubynska, M. Polutrenko, N. Kozan, *J. Ecolog. Eng.* **23** No 9, 18 (2022) https://doi.org/10.12911/22998993/150648.
5. V. Lopushniak, H. Hrytsuliak, V. Gamayunova, N. Kozan, E. Zakharchenko, Y. Voloshin, Hyna Lopushniak, Myroslava Polutrenko Y. Kotsyubynska, *J. Ecolog. Eng.* **23** No 4, 33 (2022) https://doi.org/10.12911/22998993/146268.
6. C. Hui, Y. Zhang, X. Ni, Q. Cheng, Y. Zhao, Y. Zhao, L. Du, H. Jiang, *J. Hazardous Mater.* **406**, 124650 (2021) https://doi.org/10.1016/j.jhazmat.2020.124650.
7. M. Liaskovska, *Adsorption Properties of Magnetic $CoFe_2O_4$ Based Spinel Nanoparticles.* In *Nanomaterials and Nanocomposites, Nanostructures, and Their Applications*, **253** (Eds. by O. Fesenko, L. Yatsenko) (Springer Proceedings in Physics, Springer, Cham: 2024).

https://doi.org/10.1007/978-3-031-67519-5_13
8. M. Gheju, *Water, Air, & Soil Pollution* **222** No 1, 103 (2011) https://doi.org/10.1007/s11270-011-0812-y.
9. A.O. Kotsyubynsky, V.V. Moklyak, I.M. Fodchuk, V.O. Kotsyubynsky, P.M. Lytvyn, A.B. Grubyak, *Metallofiz. Noveishie Tekhnol.* **41** No 4, 529 (2019) https://doi.org/10.15407/mfint.41.04.0529.
10. A.G. Niculescu, C. Chircov, A.M. Grumezescu, *Methods* **199**, 16 (2022) https://doi.org/10.1016/j.ymeth.2021.04.018.
11. I. Mironyuk, V. Kotsyubynsky, I. Mykytyn, Y. Kotsyubynska, V. Boychuk, V. Fedoriv, *J. Nano- Electron. Phys.* **13** No 6, 06023 (2021) https://doi.org/10.21272/jnep.13(6).06023.
12. O. Butenko, V. Boychuk, B. Savchenko, V. Kotsyubynsky, V. Khomenko, V. Barsukov, *Mater. Today: Proc.* **6**, 270 (2019) https://doi.org/10.1016/j.matpr.2018.10.104.
13. M. Polutrenko, Y. Fedorovich, H. Hrytsulyak, A. Kotsyubynsky, *Ecol. Eng. Environ. Technol.* **23** (2022).
14. D. Kasiyanchuk, E. Kuzmenko, T. Chepurna, I. Chepurnyj, *East.-Eur. J. Enterprise Technol.* **1** No 10(79), 18 (2016) https://doi.org/10.15587/1729-4061.2016.59687.
15. D.O. Lynnyk, H.M. Hrytsuliak, A.O. Kotsyubynsky, T.M. Marych, O.V. Bodnarchuk, *18th International Conference Monitoring of Geological Processes and Ecological Condition of the Environment* (Vol. 2025, No. 1, pp. 1-5). *European Association of Geoscientists & Engineers* (2025) https://doi.org/10.3997/2214-4609.2025510139.
16. V. Fedoriv, S. Bagriy, I. Piatkovska, Y. Femyak, A. Trubenko, *18th International Conference on Geoinformatics-Theoretical and Applied Aspects* (Vol. 2019, No. 1, pp. 1-5). *European Association of Geoscientists & Engineers* (2019).

Застосування наночастинок заліза для відновлення хрому

Andrew Kotsyubynsky[1], Halyna Hrytsuliak[1], Mariia Liaskovska[1,2], Vasyl Vytvytskyi[1], Oleg Turchyn[1], Yulia Kotsyubynska[2], Natalia Kozan[2], Hanna Ersteniuk[2]

[1] *Ivano-Frankivsk National Technical University of Oil and Gas, Ivano-Frankivsk, Ukraine*
[2] *Ivano-Frankivsk National Medical University, Ivano-Frankivsk, Ukraine*

Забруднення ґрунту хромом становить серйозну загрозу для навколишнього середовища та здоров'я людини через його токсичність та стійкість. Це дослідження оцінює ефективність залізовмісних наночастинок для ремедіації ґрунтів, забруднених хромом. Синтезовано та досліджено два типи наночастинок заліза: нанорозмірне нульвалентне залізо (nZVI) та наномагнетит (nFe_3O_4). Зразки ґрунту змішували з наночастинками в різних дозах, гомогенізували та інкубували в контрольованих умовах протягом 10, 20, 30, 60 та 90 днів. Для кожного часу відбору проб аналізували концентрацію хрому та його вилуговування. Хімічний та фазовий аналіз складу досліджували за допомогою рентгенівської дифракційної спектроскопії, атомно-абсорбційної спектроскопії та рентгенофлуоресцентного аналізу. Обробка обома типами наночастинок заліза показала значне зниження концентрації Cr у водних екстрактах порівняно з контрольними зразками. Вилуговування Cr в оброблених зразках ґрунту також значно знизилося та залишалося стабільним протягом усього експерименту. Результати вказують на те, що nZVI іммобілізував Cr шляхом адсорбції Cr(VI) на оболонці з його відновленням до Cr(III). Механізм взаємодії між nFe_3O_4 та Cr(VI) включав як адсорбцію [1], так і відновлення, хоча його відновна здатність була нижчою, ніж у nZVI. Аналітичні методи підтвердили зміну хімічного складу ґрунту після обробки та відділення наночастинок заліза. Це дослідження демонструє, що наночастинки, що містять залізо, можуть ефективно відновлювати забруднені хромом ґрунти за різних умов навколишнього середовища.

Ключові слова: Магнетит, Відновлення хрому, Забруднення ґрунту, Нульвалентне залізо, Нановідновлення.